

CHARACTERISING MULTIDIRECTIONAL LAMINATES UNDER TENSION/COMPRESSION-SHEAR LOADING USING A MODIFIED ARCAN FIXTURE

T. Laux^{1*}, K.W. Gan², J.M. Dulieu-Barton^{1,3} and O.T. Thomsen^{1,3}

¹ Faculty of Engineering and Physical Sciences, University of Southampton, Southampton, UK

² University of Southampton Malaysia, Johor, Malaysia

³ University of Bristol, Bristol Composites Institute (ACCIS), Bristol, UK

* t.laux@soton.ac.uk

Keywords: Multidirectional laminates, Multiaxial loading, Modified Arcan Fixture (MAF)

ABSTRACT

An experimental procedure is devised based on a re-designed Modified Arcan Fixture (MAF) that can be used to investigate composite laminates subjected to combined tension-shear and compression-shear loading. Experimental results for three multidirectional, quasi-isotropic carbon/epoxy laminates made from unidirectional plies with different thicknesses and fibre orientation angles are presented. Significant ply thickness and ply orientation effects on failure initiation, damage evolution and ultimate failure are observed. The multiaxial experimental data obtained for different laminate configurations provides a means of benchmarking and developing novel high-fidelity modelling techniques which are needed for the design and classification of next generation lightweight composite structures.

1 BACKGROUND AND MOTIVATION

Multidirectional (MD) composite laminates made from unidirectional (UD) fibre reinforced polymers are widely used in lightweight structures subjected to complex multiaxial loading. State-of-the-art modelling techniques typically adopted to predict failure initiation and damage progression in MD laminates are based on Finite Element (FE) analyses that can include material nonlinearity [1], multiple failure initiation functions [2], progressive damage models [3] and cohesive zones [4], or on more advanced frameworks such as extended FE [5] as well as on analytical tools [6]. Due to the lack of reliable multiaxial experimental data in the open literature [7], these models are generally insufficiently validated for cases of complex combined stress states. Furthermore, additional complexity to predict failure in multidirectional laminates stems from significant phenomena such as ply thickness effects [8] and ply orientation effects [9], which have been observed in uniaxial open-hole tension and compression tests [10]. There is a clear need for improved understanding of such effects under more complex combined load cases to increase confidence in composite materials and to remove the barrier to an efficient use of composites across industries. In the paper a new experimental procedure is presented that is capable of producing high-quality and repeatable experimental data for MD laminates based on a re-designed Modified Arcan Fixture (MAF) [11]. The rig has the capability to subject carbon/epoxy laminates to both combined tension-shear and compression-shear loading. Experimental data for three quasi-isotropic carbon/epoxy MD laminates with thick (300g/m²) and thin (150 g/m²) plies as well as different fibre orientation angles were obtained.

2 MATERIAL SYSTEMS

Three MD quasi-isotropic laminates, as shown in Fig. 1, made from out-of-autoclave UD carbon/epoxy prepregs were tested.

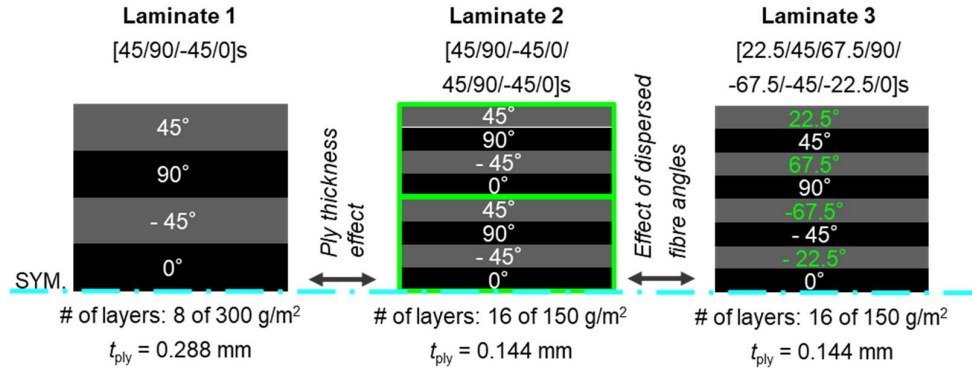


Figure 1: The quasi-isotropic carbon/epoxy laminates tested on the MAF.

The lay-ups were chosen to challenge current composite material models, as well as to establish design guidelines for MD laminates. Laminate 1 and 2 consist of plies orientated at standard fibre orientation angles, 0°, 90° and +/- 45°. The plies of Laminate 1 are approximately twice the areal weight (300g/m²) of the plies in Laminates 2 and 3 (150 g/m²), meaning the plies in Laminate 1 are almost twice as thick as in Laminate 2 and 3. Hence, the effect of ply thickness [8] on the failure behaviour of MD laminates subjected to combined tension/compression-shear loading can be assessed. Further, to study the effect of ply orientation on the failure behaviour [9] in combined tension/compression-shear, Laminate 3 comprises more dispersed and non-standard fibre angles (*e.g.* additional +/- 22.5° and +/- 67.5°).

3 EXPERIMENTAL PROCEDURE

The re-designed Modified Arcan Fixture (MAF) is shown in Fig. 2 and is based on the MAF presented in [11].

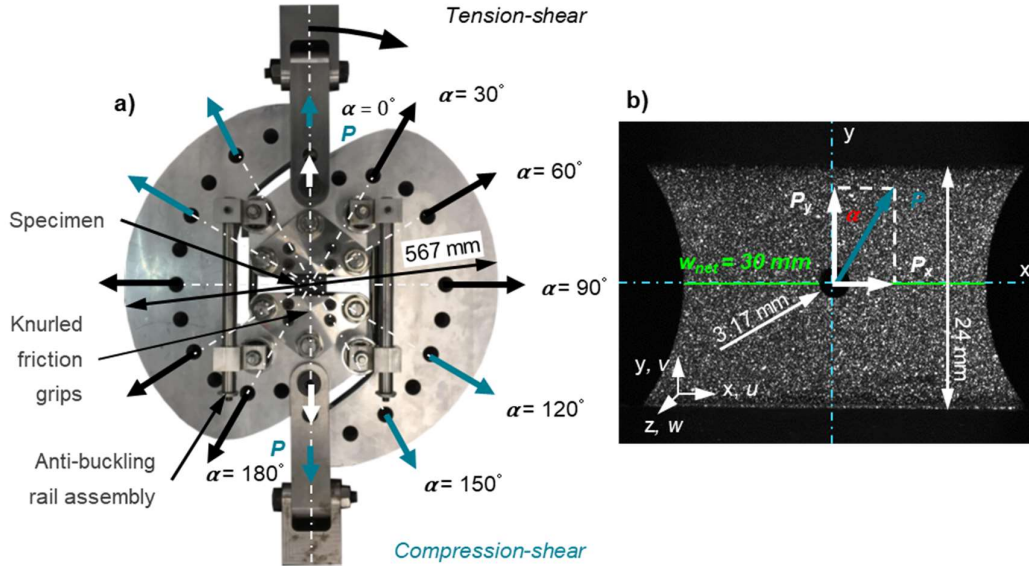


Figure 2: (a) The re-designed Modified Arcan Fixture (MAF), and how different combined tension/compression-shear loading can be induced in the specimen by the choice of the loading hole pair designated by the loading angle α ; (b) The lightly waisted open-hole specimen with the representative gauge section (green line).

The re-design successfully overcame the limitations of the MAF established in [11], where specimens failed prematurely due to tab debonding and bolt shear out failure caused by deficiencies in the grip design. A key feature of the MAF concept is the anti-buckling rail assembly that enables the application of compression-shear loading by restricting out-of-plane displacements of the fixture, which is not possible using a conventional Arcan rig [12]. By varying the loading hole pair, as shown in Fig. 2 a, different combined tension/compression-shear stress states can be induced in the specimen shown in Fig. 2 b, ranging from uniaxial tension ($\alpha = 0^\circ$) to tension-shear ($\alpha = 15^\circ - 75^\circ$), to pure shear ($\alpha = 90^\circ$), to compression-shear ($\alpha = 105^\circ - 165^\circ$) and to uniaxial compression ($\alpha = 180^\circ$).

The test specimens were of a 'lightly waisted' configuration with a central hole as shown in Fig. 2 b. Damage in MD composites made from UD plies typically initiates at stress concentrations, due to geometrical discontinuities such as notches and holes, or due to material discontinuities such as defects. Damage then grows in many cases along geometrical features of the laminate, *e.g.* delamination will grow on planes between individual plies and inter fibre matrix cracks will grow, constrained by the neighbouring fibres, along the fibre direction. Hence damage will not necessarily progress along the most severely stressed cross-section but follows, instead, the layered and orientated features of the laminate [3]. This makes the design of specimens for characterisation of MD composites difficult as a reduced or waisted gauge section will not ensure a meaningful assessment of the load carrying capability of a laminate. Further, it is difficult to identify an ideal specimen design which is suitable for all load combinations, as the specific load cases will influence the severity and location of the stress concentrations that will initiate failure. One way of overcoming some of the issues is to use an artificial stress raiser such as a small hole to initiate failure in a preferable location [13]. Hence the specimen design is based on a combination of a butterfly specimen typically used for Arcan type tests [12] and an open-hole specimen as shown in Fig. 2 b, so that failure initiates at the centre of the gauge area.

To compare the test results obtained for all load cases and laminate configurations, the specimens were treated as "structural components" from which representative failure envelopes based on the mean stresses at the waisted section (normal stress, $\overline{\sigma_{yy}}$ – shear stress, $\overline{\tau_{yx}}$) were derived. Firstly, the mean

traction, T , acting on the representative minimum gauge section (green line in Fig. 2 b), is defined in terms of the load, P , the representative net cross section width, w_{net} , and the specimen thickness, t , as:

$$T = \frac{P}{w_{net}t} \quad (1)$$

The representative combined mean stress state in the specimen net cross section is then defined in terms of the traction, T , and the loading angle, α , as:

$$\bar{\sigma}_{yy} = \frac{P}{w_{net}t} \cos(\alpha) = T \cos(\alpha) \quad (2)$$

$$\bar{\tau}_{yx} = \frac{P}{w_{net}t} \sin(\alpha) = T \sin(\alpha) \quad (3)$$

Stereo Digital Image Correlation (DIC) [14] was used in combination with the MAF on one side of the specimen to obtain the full field displacement and strain maps. The horizontal and vertical in-plane displacements are denoted as u and v respectively and the out-of-plane displacements as w . The in-plane normal, ϵ_{xx} and ϵ_{yy} , and shear strains, γ_{yx} , are then derived from the displacement fields. The full-field displacement and strain maps are used to ensure that the specimens are deformed correctly, as well as to identify the initial failure sites and subsequent damage evolution. It should be noted that ‘‘initial failure’’ is defined as the first damage event that can be observed on the surface of the specimens using DIC. Micro-cracking of the matrix has likely taken place leading up to the identified initial failure load.

4 EXPERIMENTAL RESULTS

4.1 Initial failure and damage evolution

Based on the displacement and strain maps obtained using stereo DIC, two distinct failure initiation types can be identified, *i.e.* Type 1 and 2. Example DIC maps for initial failure Type 1 are shown in Fig. 3, where delamination failure around the open hole is associated with a sudden local change in the out-of-plane (w -) displacement map. Due to confidentiality reasons the loads are normalised using the uniaxial tensile failure load of Laminate 1, $P_{LAM 1 \alpha=0}^{ult}$.

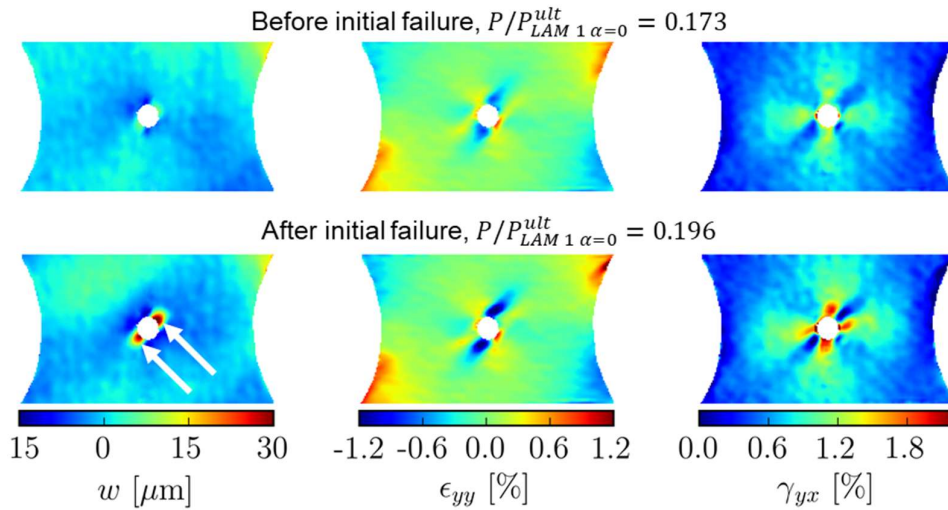


Figure 3: Type 1 failure initiation mode: delamination failure around the hole characterised by a sudden local out-of-plane displacement change (see white arrows). Shown in this example is Laminate 1 loaded in pure shear ($\alpha = 90^\circ$).

Example DIC maps for initial failure Type 2 are shown in Fig. 4, where matrix cracks in the surface ply originating from the hole and the curved edges of the specimen are associated with the appearance of local strain concentrations in the shear, γ_{yx} , and normal, ϵ_{yy} , strain maps.

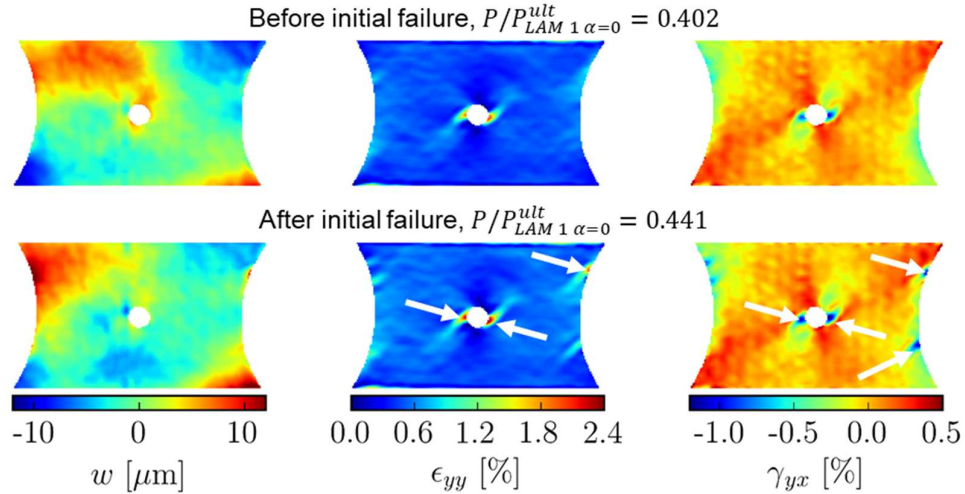


Figure 4: Type 2 failure initiation mode: matrix cracking in the $+45^\circ$ surface ply at the hole and the specimen edge (see white arrows). Shown in this example is Laminate 1 loaded in uniaxial tension ($\alpha = 0^\circ$).

The initial failure envelopes ($\overline{\sigma_{yy}^{ini}} - \overline{\tau_{yx}^{ini}}$) are obtained using Equations 1 to 3 based on the initial normalised failure load identified by the DIC as shown in Figs. 3 and 4. The failure envelopes are plotted in Fig. 5 for $\alpha = 0^\circ, 15^\circ, 90^\circ, 165^\circ$ and 180° . For the tension dominated load cases, the specimens fail in Type 2 (Pcrack), while with an increasing shear stress component the initial failure mode transitions to Type 1 (Pdel).

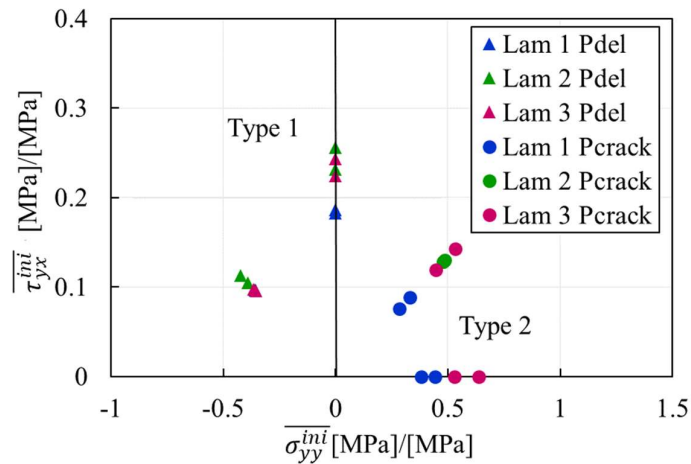


Figure 5: Mean initial representative failure envelopes. The stresses are normalised with respect to the ultimate normal stress sustained by specimens made of Laminate 1.

4.2 Ultimate failure

Table 1 illustrates the different ultimate failure modes observed as a function of the loading angle, α , and the laminate configurations.



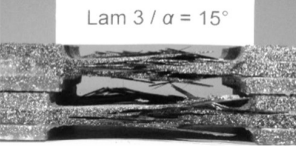
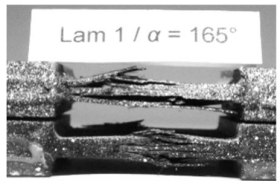
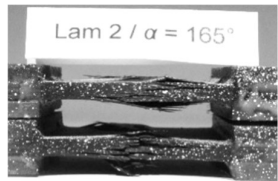
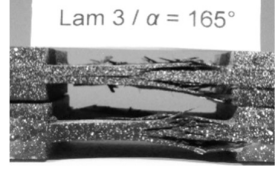
	Laminate 1	Laminate 2	Laminate 3
Tension-shear $\alpha = 15^\circ$	 <p>Lam 1 / $\alpha = 15^\circ$</p> <p>Delamination dominated failure</p>	 <p>Lam 2 / $\alpha = 15^\circ$</p> <p>“Fibre pull-out” failure [10]</p>	 <p>Lam 3 / $\alpha = 15^\circ$</p> <p>No “complete” break</p>
Compression-shear $\alpha = 165^\circ$	 <p>Lam 1 / $\alpha = 165^\circ$</p> <p>“Crushing”</p>	 <p>Lam 2 / $\alpha = 165^\circ$</p> <p>“Crushing”</p>	 <p>Lam 3 / $\alpha = 165^\circ$</p> <p>[22.5°/0°/0°/22.5°] plies form central wedge</p>

Table 1: Examples of representative specimens failed in tension-shear (top) and compression-shear (bottom).

For tension-shear loading (Table 1, top row), the three laminates exhibit significantly different ultimate failure patterns. The ply thickness effect is apparent between Laminates 1 and 2, where extensive delamination failure is predominant in Laminate 1 due to its thicker plies, whereas failure in the Laminate 2 mainly is due to fibre/ply pull-out. The change of ultimate failure mode due to the ply thickness effect was also observed by Hallett *et al.* [10] in uniaxial open-hole tension tests. The thin ply non-standard Laminate 3 shows the influence of the stacking sequence on the ultimate failure mode. Different to Laminates 1 and 2, the Laminate 3 specimens did not break completely into two, with the +22.5° and 0° fibres left partly intact. For compression-shear loading (Table 1, bottom row), the failure modes/patterns of Laminate 1 and 2 are similar. However, for Laminate 3, the relatively stiff (in the direction of the compressive normal load) [22.5°/0°/0°/22.5°] central sub-laminate cluster acts as a wedge separating the outer sub-laminates and thus “opens” the laminate under compressive loading.

The mean ultimate failure envelopes ($\overline{\sigma_{yy}^{ult}} - \overline{\tau_{yx}^{ult}}$) were obtained from Equations 1 to 3 using the normalised maximum measured loads. The failure envelopes are plotted in Fig. 6 for $\alpha = 0^\circ, 15^\circ, 90^\circ, 165^\circ$ and 180° .

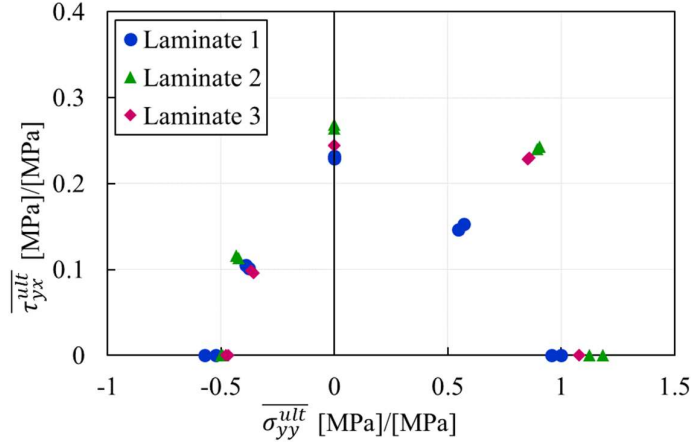


Figure 6: Mean ultimate representative failure envelopes. The stresses were normalized with respect to the ultimate normal stress sustained by specimens made of Laminate 1.

It is observed that the specimens made from Laminates 2 and 3 are significantly stronger (up to a factor of 1.5) than Laminate 1 when subjected to combined tension-shear loading. Assuming that failure is driven by initial transverse cracking, which eventually leads to delamination and fibre failure [10], the difference can be explained by the in-situ strength effect [8]. This means the in-situ transverse tensile and shear strengths are higher for thin plies than for thick plies, so that the damage onset is delayed in Laminate 2 and 3 in comparison to Laminate 1, resulting in a higher ultimate strength. For compression-shear loading, the differences between the laminate mean strengths are small. This result shows that the transverse compressive strength of the UD plies is not significantly affected by the ply thickness in contrast to the transverse tensile and shear strengths, where the opposite is the case. Furthermore, Laminate 2 is consistently stronger for all loading angles than Laminate 3 with an average difference of 9%. This can be explained by the observation that the in-situ effect not only depends on the ply thickness but also on the constraining effect of neighbouring plies which is controlled by the relative fibre orientation angle difference [9]. The larger the relative angle between plies, the larger is the constraining effect, which leads to higher in-situ strengths in Laminate 2 compared to Laminate 3.

5 CONCLUSIONS AND OUTLOOK

An experimental procedure based on a re-designed Modified Arcan Fixture (MAF) has been devised. The procedure was successfully used to characterise the initial and ultimate strength of specimens made from three different quasi-isotropic carbon/epoxy MD laminates. The three laminates feature different ply thicknesses, different number of plies and different fibre orientation angles. The following guidelines for the design of MD laminates subjected to combined tension/compression-shear loading can be derived:

- For combined tension-shear loading, the strength increase of up to 150% resulting from the use of thinner plies, but with a higher total number of plies, justifies the additional manufacturing cost of Laminate 2 and 3 over Laminate 1.
- For combined compression-shear loading, the use of the thinner plies does not significantly improve the laminate strength in comparison to the thick ply Laminate 1. Therefore, the additional manufacturing cost of using thinner plies is not necessarily justified in all cases.

- The use of non-standard fibre orientation angles ($\pm 22.5^\circ$ and $\pm 67.5^\circ$) is not assessed to be beneficial based on the experimental data obtained. The additional manufacturing cost and increased wastage associated with the non-standard ply angles is unlikely to be justifiable.

Future work is focused on the Finite Element simulation of the tested laminate configurations subjected to combined tension/compression-shear loading. To achieve this, the specimens will be modelled at the meso-scale level using a single layer of solid elements for each UD ply. The constitutive model adopted for the plies will be based on the continuum damage model proposed by Maimí et al. [3]. Failure activation functions based on the LaRC03 failure criterion [2] will be used to predict the different intra ply failure mechanisms of UD fibre reinforced composites, while also accounting for the in-situ strength effect [15]. Moreover, interlaminar failure (delamination) is modelled using cohesive surfaces [4]. Current on-going work is focused on assessing the agreement between the experimental observations and the numerical predictions with the aim of establishing the maturity of current modelling approaches for advanced composite materials.

ACKNOWLEDGEMENTS

This work is supported by EPSRC under the Doctoral Training Grant 1801230 and through a Stanley Gray Fellowship granted to the presenting author by the Institute of Marine Engineering, Science and Technology (IMarEST). The presenting author also thanks Professor P.P. Camanho and his team for supporting a four weeks placement at the Faculdade de Engenharia (FEUP), Universidade do Porto.

REFERENCES

- [1] G. M. Vyas, S. T. Pinho, and P. Robinson, "Constitutive modelling of fibre-reinforced composites with unidirectional plies using a plasticity-based approach," *Compos. Sci. Technol.*, vol. 71, no. 8, pp. 1068–1074, 2011.
- [2] C. G. Davila, P. P. Camanho, and C. A. Rose, "Failure criteria for FRP laminates," *J. Compos. Mater.*, vol. 39, no. 4, pp. 323–345, 2005.
- [3] P. Maimí, P. P. Camanho, J. A. Mayugo, and C. G. Davila, "A continuum damage model for composite laminates: Part I - Constitutive model," *Mech. Mater.*, vol. 39, no. 10, pp. 897–908, 2007.
- [4] P. P. Camanho, C. G. Davila, and M. M.F., "Numerical Simulation of Mixed-mode Progressive Delamination in Composite Materials," vol. 37, no. 16, 2003.
- [5] R. Higuchi, T. Okabe, and T. Nagashima, "Numerical simulation of progressive damage and failure in composite laminates using XFEM/CZM coupled approach," *Compos. Part A Appl. Sci. Manuf.*, vol. 95, pp. 197–207, 2017.
- [6] C. Furtado, A. Arteiro, M. A. Bessa, B. L. Wardle, and P. P. Camanho, "Composites : Part A Prediction of size effects in open-hole laminates using only the Young 's modulus , the strength , and the R -curve of the 0 ° ply," *Compos. Part A*, vol. 101, pp. 306–317, 2017.
- [7] M. Hinton, A. Kaddour, and P. D. Soden, *Failure criteria in fibre-reinforced polymer composites*. Elsevier, 2004.
- [8] A. Parvizi, K. W. Garrett, and J. E. Bailey, "Constrained cracking in glass fibre-reinforced epoxy cross-ply laminates," *J. Mater. Sci.*, vol. 13, no. 10, pp. 2131–2136, 1978.
- [9] D. L. Flaggs, "Experimental determination of the in situ transverse lamina strength in graphite / epoxy laminates," *J. Compos. Mater.*, vol. 16, pp. 103–116, 1982.
- [10] S. R. Hallett, B. G. Green, W. G. Jiang, and M. R. Wisnom, "An experimental and numerical investigation into the damage mechanisms in notched composites," *Compos. Part A Appl. Sci. Manuf.*, vol. 40, no. 5, pp. 613–624, 2009.
- [11] K. W. Gan, T. Laux, S. T. Taher, J. M. Dulieu-Barton, and O. T. Thomsen, "A novel fixture for determining the tension/compression-shear failure envelope of multidirectional composite laminates," *Compos. Struct.*, vol. 184, no. August 2017, pp. 662–673, 2018.
- [12] M. Arcan, Z. Hashin, and A. Voloshin, "A method to produce uniform plane-stress states with applications to fiber-reinforced materials," *Exp. Mech.*, vol. 18, no. 4, pp. 141–146, 1978.
- [13] S. R. Hallett, B. G. Green, W. J. Kin, H. Cheung, and M. R. Wisnom, "The open hole tensile

- test : a challenge for virtual testing of composites,” *Int. J. Fract.*, vol. 158, pp. 169–181, 2009.
- [14] M. A. Sutton, J. J. Orteu, and H. Schreier, *Image correlation for shape, motion and deformation measurements*. Springer, 2009.
- [15] P. P. Camanho, C. G. Davila, S. T. Pinho, L. Iannucci, and P. Robinson, “Prediction of in situ strengths and matrix cracking in composites under transverse tension and in-plane shear,” *Compos. Part A Appl. Sci. Manuf.*, vol. 37, no. 2, pp. 165–176, 2006.